

Registration of different phases of contrast-enhanced CT/MRI data for computer-assisted liver surgery planning: Evaluation of state-of-the-art methods

T Lange, T H Wenckeback, H Lamecker, M Seebass, M Hünerbein, S Eulenstein, B Gebauer, P M Schlag

T Lange, M Hünerbein, S Eulenstein and P M Schlag

Department of Surgery and Surgical Oncology, Charité – University Medicine Berlin, Germany

H Lamecker and M Seebass

Zuse Institute Berlin, Germany

T H Wenckeback

Zuse Institute Berlin and Department of Computer Science, Humboldt-University of Berlin, Germany

B Gebauer

Department of Radiotherapeutics, Charité – University Medicine Berlin, Germany

Correspondence to: T Lange, E-mail: lange_t@charite-buch.de

Abstract

The exact localization of intrahepatic vessels in relation to a tumour is an important issue in oncological liver surgery. For computer-assisted preoperative planning of surgical procedures high quality vessel models are required. In this work we show how to generate such models on the basis of registered CT or MRI data at different phases of contrast agent propagation.

We combine well-established intensity-based rigid and non-rigid registration approaches using Mutual Information as distance measure with different masking strategies as well as intensity inhomogeneity correction for MRI data. Non-rigid deformations are modelled by multilevel cubic B-splines. Quantitative evaluations of 5 MRI and 5 CT image pairs show that the liver moves rigidly 7.2 (+/- 4.2) mm on average, while the remaining non-rigid deformations range from 1.4–3 mm. As a result we find that masked rigid registration is necessary and in many cases also sufficient on clinical data. After non-rigid registration the matching shows no deviations in most cases.

Keywords: Computer-aided surgery, liver, vascular networks, rigid and non-rigid, registration, inhomogeneity correction, automatic masking

Paper accepted:

Published online: Available from: www.roboticpublications.com

DOI: 10.1581/mrcas.2005.010302

INTRODUCTION

Surgical removal of primary tumours and metastases from the liver is a potentially curative therapy. The location of the tumour in relation to the vascular system of the liver has a strong influence on the operability decision and resection strategy. High quality geometric computer models of the liver tissue as well as the vascular system may support the surgeon in planning and implementing liver resections. They can provide precise resection

proposals⁽¹⁾, guide intraoperative procedures^(2, 3) and improve tumour detection (Figure 1). One way to obtain high quality models of the portal and hepatic veins – suitable for such tasks – is by registration of different phases of CT or MRI data. The planning procedure is based on preoperative CT or MRI data under contrast agent injection.

In this work we present a method to generate high quality vessel models containing portal as well as hepatic veins via registration of different phases of

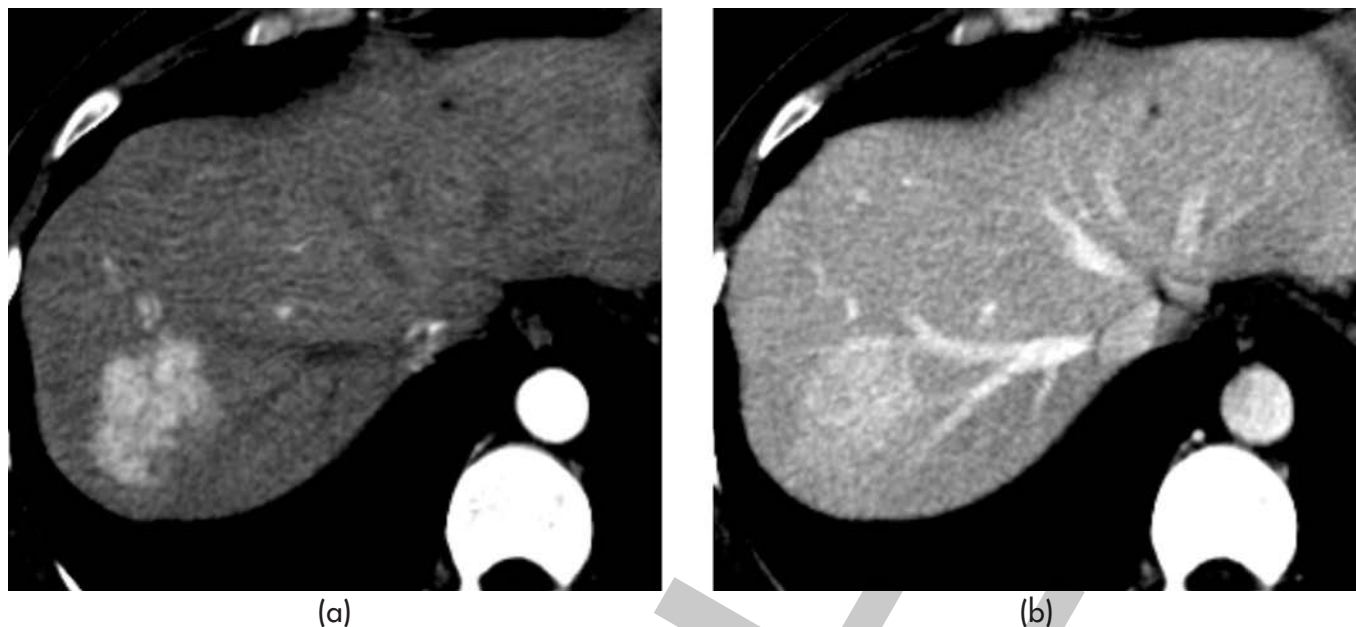


Figure 1 The boundary of the tumour is well demarcated in the PV phase (left), while the vascular system has higher contrast in the HV phase (right).

contrast-enhanced CT and MRI data. The focus is on the evaluation of state-of-the-art registration methods on clinical data and not on the development of new algorithms.

Clinical background

An important prerequisite for successful oncological liver surgery is the complete resection of the tumour with a safety margin of about one centimetre in order to prevent recurrent tumours. A golden rule states that the surgeon must not see the tumour during surgical intervention. Resections based on the extent of the tumour only (including safety margin) are called “atypical”. Only in case of small tumours lying close beneath the liver surface, should atypical resections be performed. In all other cases, the spatial relation of the tumour to the vascular system of the liver has to be taken into account (“anatomical resection”).

In contrast to many other organs, the liver possesses not only arteries and veins, but also a third blood vessel system, the portal veins. They drain venous blood from the entire gastrointestinal tract, thus supplying eighty percent of the liver’s blood. For an anatomical resection, first vessel branches lying inside the safety margin as well as their dependent branches have to be identified. Next the liver tissue supplied by these branches (called a vascular territory) has to be determined.

Consequently, a whole segment of the liver must be removed rather than the tumour on its own.

Planning systems

Motivated by strong anatomical variations of the liver’s vascular system, several groups^(4–7) are developing software systems that allow for precise surgery planning. Those facilities support the surgeon in deciding whether a resection is feasible or not, and in specifying the resection strategy. Planning is always based on 3D surface models derived from segmented vessels, liver tissue and tumours from contrast-enhanced CT or sometimes MRI data.

One aim of planning systems is to visualize the exact location of the tumour in relation to the vessels in 3D, and to measure distances and volumes. Based on the 3D models, the surgeon decides which vessel branches can be preserved.

Another functionality are automated resection proposals containing the dependent vascular territories. Typically, only the portal veins are considered in the computation. This is justified by the fact that hepatic arteries are supposed to run close to the portal veins; they are difficult to identify. However, with modern multi-slice CTs arteries can also be imaged.

An important issue is to ensure not only blood supply but also blood drainage via the hepatic veins.

Preim et al. ⁽¹⁾ were the first to incorporate hepatic veins in the planning process.

Image acquisition using contrast agents

In contrast-enhanced bi- or tri-phase imaging, two or three acquisitions are carried out at different points in time depending on the arrival time of the contrast agent in arteries, portal and hepatic veins. First, the contrast agent reaches the arteries (arterial phase), then the portal veins (portal venous phase) and at last the hepatic veins (hepatic venous phase). In the portal venous (PV) phase, the hepatic veins are not enhanced. However, in the hepatic venous (HV) phase, portal veins are typically also visible, but with lower contrast as in the portal venous phase. To derive high-quality vessel models, portal veins should be segmented from a PV phase and hepatic veins from a HV phase, see Figure 2. PV as well as HV images are acquired during respiration hold, which is normally at end-inspiration. Unfortunately, the patient breathes between the acquisitions - the position and shape of the liver cannot be reproduced exactly. So if segmentations of portal and hepatic veins from different phases are to be used in one common model, the phases have to be registered. Registration is the process of determining a geometrical transformation which maps each point in one data set (model) to its anatomically corresponding point in the other data set (reference).

Previous work

Several clinical applications and algorithms concerning the registration of CT or MRI data of the liver have been published. The applications range from radiosurgery ⁽⁸⁾, control of thermal ablations ⁽⁹⁾, localization of malignancies in combination with FDG-PET ⁽¹⁰⁾ to quantification of tumour volume change over time ^(11, 12). Intensity-based registration methods using Mutual Information (MI) as a similarity measure allow rigid or even non-rigid transformations to prevail. Feature-based approaches using liver vessels have also been introduced. Charnoz et al. ⁽¹²⁾ extract a graph representation of the portal vein from model and reference CT data respectively, and perform an adapted graph matching. In contrast to that, Aylward et al. ⁽¹³⁾ determine a vessel model from model data only, which is fitted directly into the intensity data of the reference. Both methods are promising, but have to be evaluated on a larger set of data.

Successful rigid and non-rigid registrations on different clinical liver data sets have been reported for intensity-based methods using MI. In case of rigid transformations, in all referenced work ⁽⁸⁻¹¹⁾ a liver mask is used to restrict the evaluation of the MI value on liver voxels. That means that the motion of the liver in relation to its surroundings has no influence on the registration result except for motion-dependent deformations of the liver itself.

Rohlfing et al. ⁽⁸⁾ as well as Park et al. ⁽¹¹⁾ apply intensity-based non-rigid registration to correct for these liver deformations. Again, a distance measure based on MI is minimized.

The most important task is to ensure that deformations are physically plausible, i.e. there exists a certain degree of smoothness. Therefore, the main characteristic of non-rigid registration methods is the underlying deformation model, and consequently the approach for numerical solution of the problem ⁽¹⁴⁾.

In parametric image registration, deformations are parameterized by appropriate basis functions, for example, cubic B-splines ⁽¹⁵⁾ or Thin-plate splines ⁽¹⁶⁾. A smooth free-form deformation is found by non-linear optimization of the configuration of B-spline control points; smoothness is an intrinsic property of cubic spline functions. Sometimes, when deformations have a highly local character, extra regularizers are employed.

In non-parametric image registration, smoothness is always introduced by a smoothing term; it is added to the distance measure thus penalizing non-smooth deformations. There are several approaches for those regularizers ⁽¹⁷⁾, which are sometimes physically motivated like in elastic ⁽¹⁸⁾ or fluid registration ⁽¹⁹⁾.

For the purpose of tumour follow-up, Park et al. ⁽¹¹⁾ apply parametric non-rigid registration based on Thin-plate splines ⁽¹⁶⁾ to CT data of the liver acquired on different days. The Thin-plate splines are defined by 24 irregularly distributed control points, which are positioned automatically. The disadvantage of Thin-plate splines is their global support. This means that each control point influences the transformation at every data point. In contrast to Thin-plate splines, B-splines are defined on a regular control grid and have local support; each control point influences only a well-defined sub volume. Moreover, a hierarchy of B-splines can be easily generated. Both aspects lead to a more efficient implementation. Rohlfing et al. ⁽⁸⁾ use such

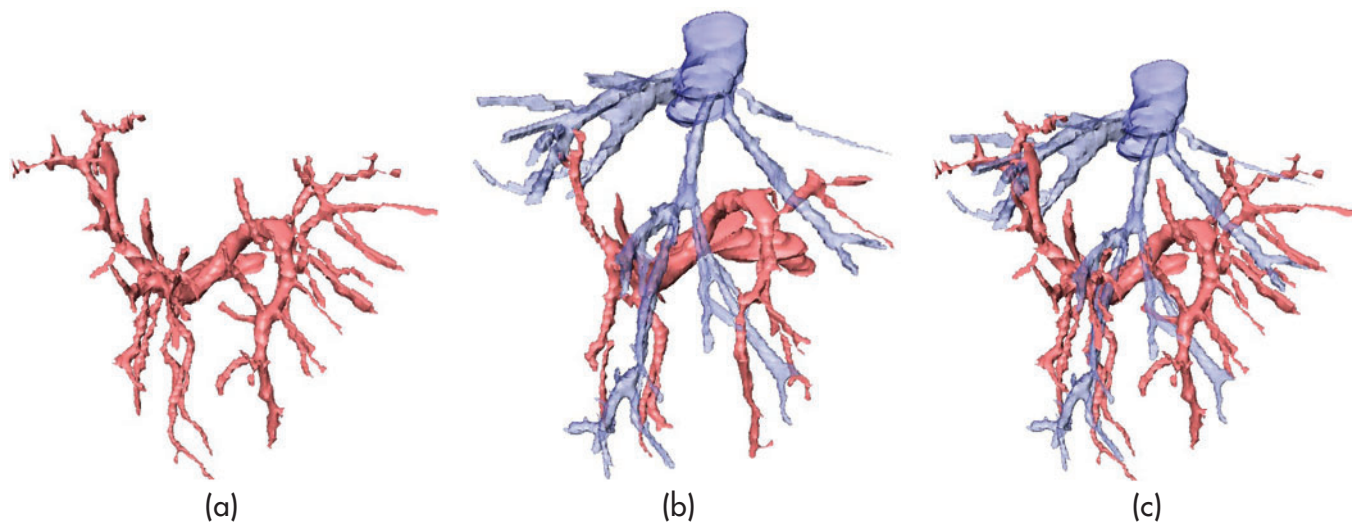


Figure 2 Portal (pink) and hepatic (blue) veins are displayed in the PV (a) and the HV (b) phase. A combination of portal veins from the PV and hepatic veins from the HV phase is visualized in (c).

a multilevel B-spline technique to build a multi-stage respiratory motion model of the liver.

Our approach

The aim of this contribution is to investigate how much the liver's position and shape changes between the portal venous and the hepatic venous phase, and whether these changes can be eliminated by rigid, and if necessary, by non-rigid MI based registration. The investigations cover CT as well as MRI data.

The influence of a manual and an automatic masking strategy on the rigid registration results is analyzed. The non-rigid registration algorithm is similar to the multilevel B-spline technique of Rohlfing et al. ⁽⁸⁾, but in case of MRI data, an intensity inhomogeneity correction is applied beforehand.

METHODS

The rigid registration method used in this work is an implementation of the popular multi-resolution algorithm of Studholme et al. ⁽²⁰⁾. The idea behind it is to minimize mutual information (MI) between model and reference image by systematically varying translation and rotation parameters of the model in relation to the reference image. In order to improve robustness and run-time, the algorithm makes use of a pyramid of low-pass filtered and resampled copies of the original image data. Optimization begins on a coarse resolution (5 mm isotropic voxel size) and successively moves on to finer levels of the pyramid until it reaches the resolution of the original data.

MI is implemented by histogram binning. In all cases, the HV phase is taken as the reference and the PV phase as the model. The initial transformation of the model data is the identity. No manual pre-registration is necessary for PV to HV phase registration.

Masking

As mentioned in the introduction it is reasonable to use a liver mask to restrict the MI evaluation to liver voxels. Different manual, semi-automatic and automatic masking methods have been used in the literature. Dalen et al. ⁽¹⁰⁾ construct a bounding box of the liver manually. Carillo et al. ⁽⁹⁾ additionally segmented the liver manually. Rohlfing et al. ⁽⁸⁾ also use a manually segmented liver mask for rigid registration, but only for comparison with their non-rigid strategy; their actual algorithm works without masking. Park et al. ⁽¹¹⁾ provide automatic masking by a probabilistic liver atlas constructed from 32 different patients.

In our application, usually a manually segmented liver mask exists anyway, since it is needed for the preoperative planning process. But in addition, we investigated an automatic method to generate a mask via an active shape model of the liver ⁽²¹⁾. The general idea to use a statistical model generated from a training set of manually segmented livers is similar to the work of Park et al. ⁽¹¹⁾, yet the method to achieve this goal is fundamentally different. The model of Park et al. is constructed by Thin-plate spline warping of each instance of the training set to

a reference data set. Each voxel of the probabilistic atlas represents the fractional percentage of warped patient data sets that have a label at that reference voxel location. For registration, the probabilistic atlas is mapped onto the reference data set and a threshold is set at its twentieth percentile. The threshold volume defines the mask.

Our shape model ⁽²²⁾ is based on surfaces generated from 43 segmented liver training data sets, but not on labelled voxels. The idea is to map all training surfaces to a common reference coordinate system, and to perform a principal component analysis on corresponding surface points ⁽²¹⁾. In order to solve the inherent correspondence problem, surface feature lines on each surface are identified semi-automatically. The surface is divided into so-called patches defined by these feature lines. Each patch of one surface is then automatically mapped to the corresponding patch on the other surface by minimizing metric distortion of the mapping. This results in a one-to-one correspondence mapping which is dense across both surfaces. Principal component analysis of corresponding surface points provides a mean shape and the main shape variations. The weights of the shape variations are parameters of the shape model. In an optimization process, the position (translation, rotation) and the shape parameters are adapted to fit the model surface to the grey value data of an individual patient data set. The adaptation is driven by evaluation of grey value profiles perpendicular to the model surface. After automatically adapting the shape model to an individual data set, the resulting liver surface is scan converted to label voxel data. These labels are then used as a liver mask.

A detailed description of the shape model, the adaptation process and the accuracy of the method is given in Lamecker et al. ^(23, 24). So far, only CT data were segmented in this fashion. A profile evaluation strategy for MRI data is subject to future work.

The influence of different masking strategies on the registration process is evaluated in the results section.

Non-rigid registration

In general, rigid registration is not able to account for all differences between the two imaged phases. Remaining non-linear deformations are treated by applying a non-rigid registration algorithm within the same parametric framework as the initial rigid alignment, where the former result is taken as input;

only the class of geometric transformations is extended to higher degrees of freedom. In this step, no masking of the liver is employed.

The deformation model is defined on a 3D discrete uniform control point grid (CPG) with cubic B-spline interpolation between adjacent control points. The scope of each control point is defined by grid resolution and decreases continuously within a sub-volume defined by its second-to-next neighbours. The algorithm starts on a very coarse grid with 100 mm grid spacing, which is successively refined to 12.5 mm spacing (3 refinements). Hence, global deformations are corrected at the beginning, while local deformations are iteratively resolved later on. Complementary, we have again a data pyramid. The main intention is to prevent the optimization from terminating in a local minimum of the distance measure. At each level of the pyramid, a gradient descent-like optimization strategy minimizes MI.

Most of the computation time is needed for evaluation of the distance measure with respect to the gradient calculation. The computational cost for approximating the gradient numerically is not dependent on grid resolution, but on image resolution. Thus, the multi-resolution strategy considerably accelerates run time as a by-product. Furthermore, these gradient computations can be easily parallelized. For our experiments, we use a multi-processor implementation for shared memory machines like in Rohlfing et al. ⁽²⁵⁾; there exists a single-processor variant for different platforms as well, with a run-time of about an hour. The tool is incorporated into AMIRA ⁽²⁶⁾ – a system for advanced visual data analysis. Moreover, all visualizations in this paper have been created using AMIRA.

Inhomogeneity correction for MR-images

In MR imaging, inhomogeneities of the magnetic fields may result in spatial variations of the image intensity, in particular, if surface coils are applied. Those intensity variations influence intensity-based non-rigid registration significantly. The algorithm introduced by Likar et al. ⁽²⁷⁾ compensates for such intensity variations by multiplying grey values with a 3D polynomial of order 4. As a measure of image homogeneity, the entropy is calculated from the grey value histogram. Entropy should be minimal for a homogeneous image, because it contains less information than an inhomogeneous image.

Application of inhomogeneity correction leads to convincing non-rigid registration results for MRI data as shown in the results section.

Evaluation methods

It is a difficult task to evaluate performance and accuracy of registration methods, and in particular of non-rigid registration methods, on real clinical data, because there is no bench-mark available for comparison. However, some validation is possible. We consider three different kinds of evaluation method:

a) Visual inspection: The first kind of evaluation is a thorough visual inspection. In order to assess vessel registration, each axial slice of the model image is overlaid with intersection lines of a vessel model segmented from the reference data. Significant distances are measured interactively. This way, only distances within axial slices are investigated, though.

b) Comparison of different registration strategies: The second kind of evaluation method simply computes differences in the transformations determined by different registration strategies. The question of whether there is a significant difference between manual, automatic or no liver masking is addressed. Centre lines of the portal veins serve as test structures; they are automatically extracted from segmented portal veins by the TEASER algorithm⁽²⁸⁾. The same centre line points are transformed with both transformations that shall be compared. Thus, corresponding points between different transformations are obtained and the distance between these points can be computed.

c) 3D distance measurements: The third kind of evaluation is an attempt to get a more objective registration error. To this end, centre lines of the portal veins extracted from PV phase are compared to centre lines extracted from HV phase. Their distance is determined by computing for each point on the centre lines in the HV phase the closest point of the centre lines extracted from PV phase. It is important to notice that the closest point is not necessarily the anatomical corresponding point, and consequently, the distance is just an approximation. Additional inaccuracies of the measurement methodology are caused by the image resolution (in particular slice thickness) and by the segmentation and centre line extraction process. Thus, the resulting distance does not reflect absolute accuracy

of the registration methods, but general tendencies like a distance decrease can be detected.

RESULTS

Image acquisition

Abdominal contrast-enhanced breath-hold CT (5 patients) and MRI (5 patients) images in PV and HV phase were acquired. The CT data were imaged on a single slice spiral scanner (GE HiSpeed) with 2 mm reconstructed slice thickness (5 mm collimation, pitch 1.5) using Imeron as contrast agent. The MR images were acquired on a 1.5 T Siemens Symphony scanner using a surface coil and Magnevist as contrast agent. A T_1 -weighted FLASH 3D VIBE sequence with fat saturation was applied. The sequence parameters were $T_E = 1.43$ ms, $T_R = 4.66$ ms, flip angle = 10° , pixel size = 0.6 mm, slice thickness = 2.5 mm, 72 axial slices.

Evaluation of different registration strategies

Visual inspection of the original data shows obvious deviations between PV and HV phase for all but two data sets (CT2, CT3). In the following, visual inspection refers to the evaluation procedure defined in the methods section. Rigid registration of the original data without masking in fact reduces distances, but is clearly not satisfactory, whereas rigid registration with masking in many cases leads to sufficient results (see Figure 3a and 3b). The reason why liver masking is so important for rigid registration is illustrated in Figure 3c and 3d. Although the liver has moved in this case, surrounding structures have not. Since image distance is measured globally, registration without masking determines a rigid transformation which is actually a compromise of the moving liver and the resting surrounding structures.

In Figure 4, portal veins extracted from the PV (transparent) and HV phase (solid) of CT1 are shown. The improvement from original over rigidly registered (with and without masking) to non-rigidly registered data is clearly visible. The quality of the results is classified into two categories. The first category contains those data sets that have minor deviations after masked rigid registration and where no deviations can be observed after non-rigid registration. This category includes data sets with few vessel segments exhibiting deviations of 1–2 mm (CT2, CT3, CT4), data sets with many segments having 1–2 mm (MR5) and data sets having some segments with 2–3 mm (MR1, MR3).

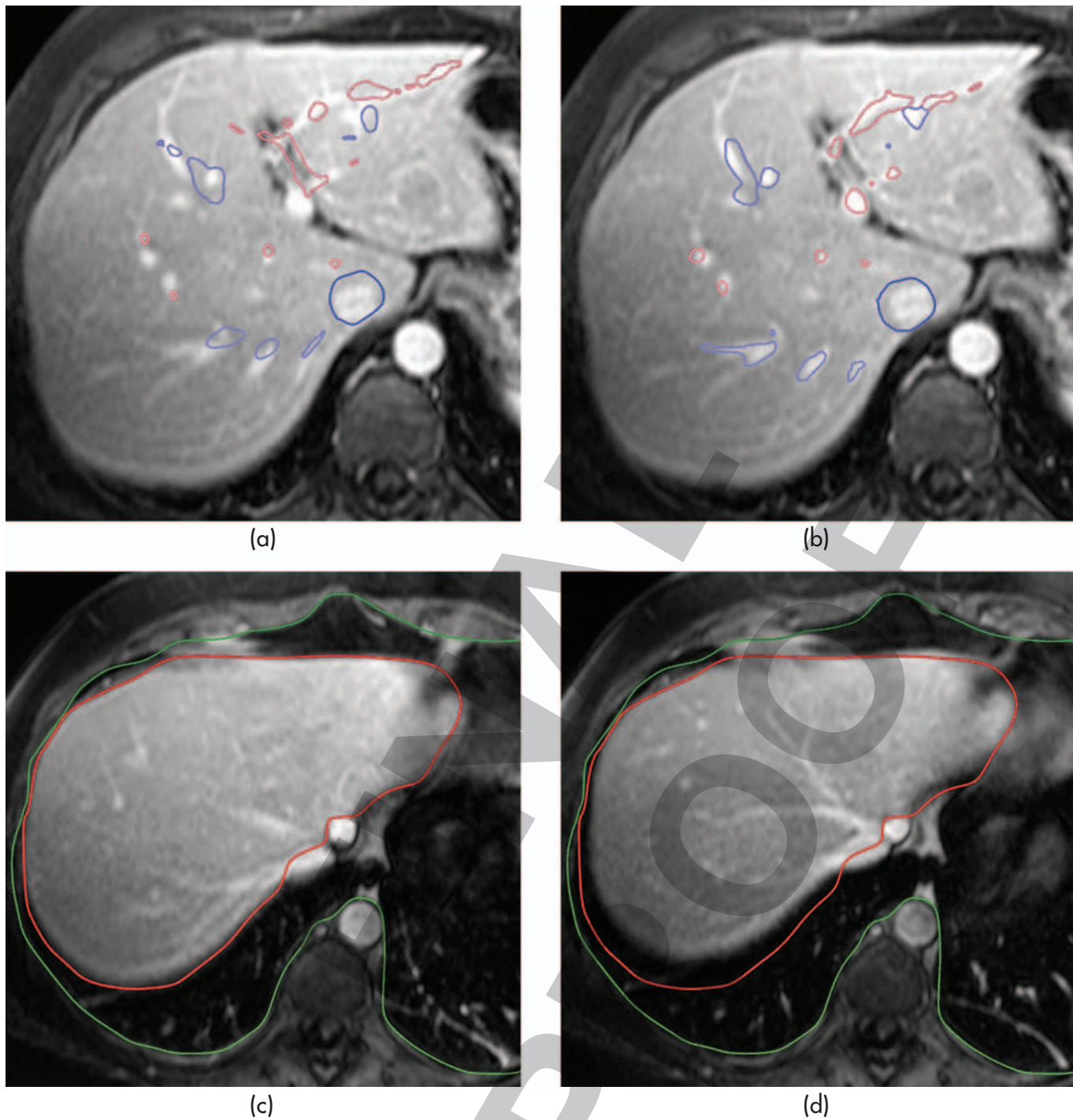


Figure 3 Rigidly registered vessels without (a) and with (b) masking are overlaid on an image slice of MR2. Original slices of the same data set in PV (c) and HV (d) phase are overlaid with outlines of the liver (red) and surrounding structures (green) extracted from PV phase.

As mentioned before, non-rigid registration completely removes these differences. The second category contains data sets having many vessel segments with 2–3 mm differences (CT1, CT5, MR2, MR4) after masked rigid registration. Non-rigid registration improves the results in those cases, but not completely. In CT1 and MR2, one single

segment with 3 mm distance and in CT5 and MR4 two segments with 2–3 mm distance are observed. All those segments are end parts of small peripheral vessels. We ascribe these differences to the fact that the vessels are small; they have a very low influence on the MI distance measure which is in this case dominated by the nearby liver surface. As the liver

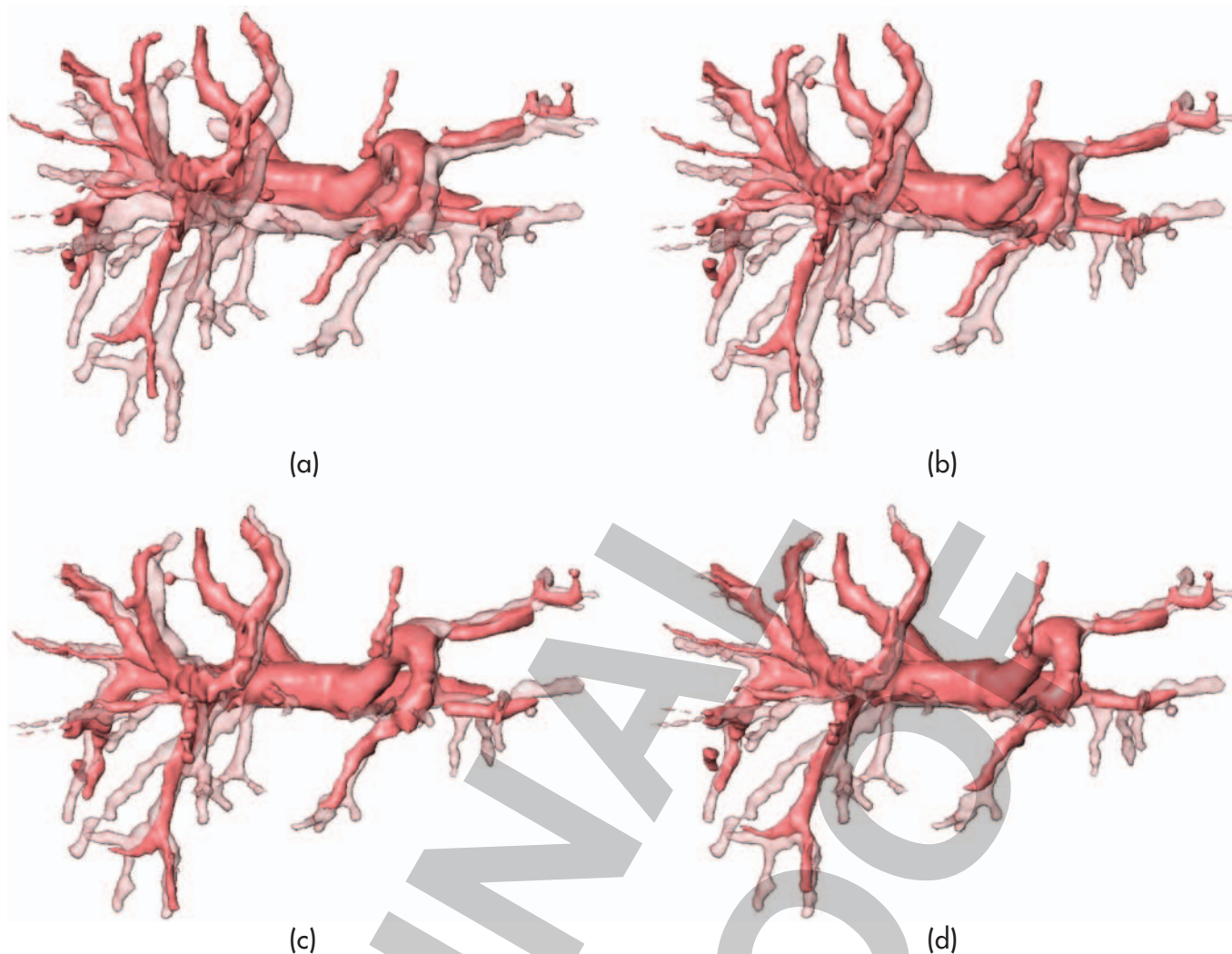


Figure 4 Portal veins are extracted from PV phase (transparent) and HV phase (solid) of CT1, whereas HV phase is shown at original position (a), rigidly registered without masking (b) rigidly registered with masking (c) and non-rigidly registered (d).

shows little structure at the periphery, local transformation is not well-defined. Results after (masked) rigid and non-rigid registration are illustrated for CT1 in Figure 5 and MR4 in Figure 6.

The analysis of differences between the computed transformations confirms the results of the visual inspection and interactive distance measurement. In Table 1, for each data set the root mean square (RMS) distance between portal vein centre line points before and after masked rigid registration is listed. The RMS distance ranges between 1.3 and 12.3 mm and is on average 7.2 (± 4.2) mm. Conforming with visual inspection, significant movements of the liver vessels are observed in all cases except for CT2 and CT3. In the second row of Table 1, differences between rigidly registered data with (manual) and without liver masking are shown.

The distances range between 0.7 and 5.9 mm and are 3.9 (± 1.9) mm on average. This confirms the influence of the masking procedure on the rigid registration process. In the last row, distances between rigidly (with manual masking) and non-rigidly registered centre lines are shown. The distances range between 1.4 and 3.0 mm and are 2.2 (± 0.6) mm on average. Again, the results of the visual inspection are approved: Data sets CT1, CT5, MR2 and MR4 exhibit the most significant non-rigid deformations.

For those three data sets showing approximately 3 mm deviations between rigid and non-rigid registration, the third evaluation method is applied (Table 2). The approximated distances between portal vein centre lines extracted from PV and HV phase are determined. A clear advantage of rigid registration

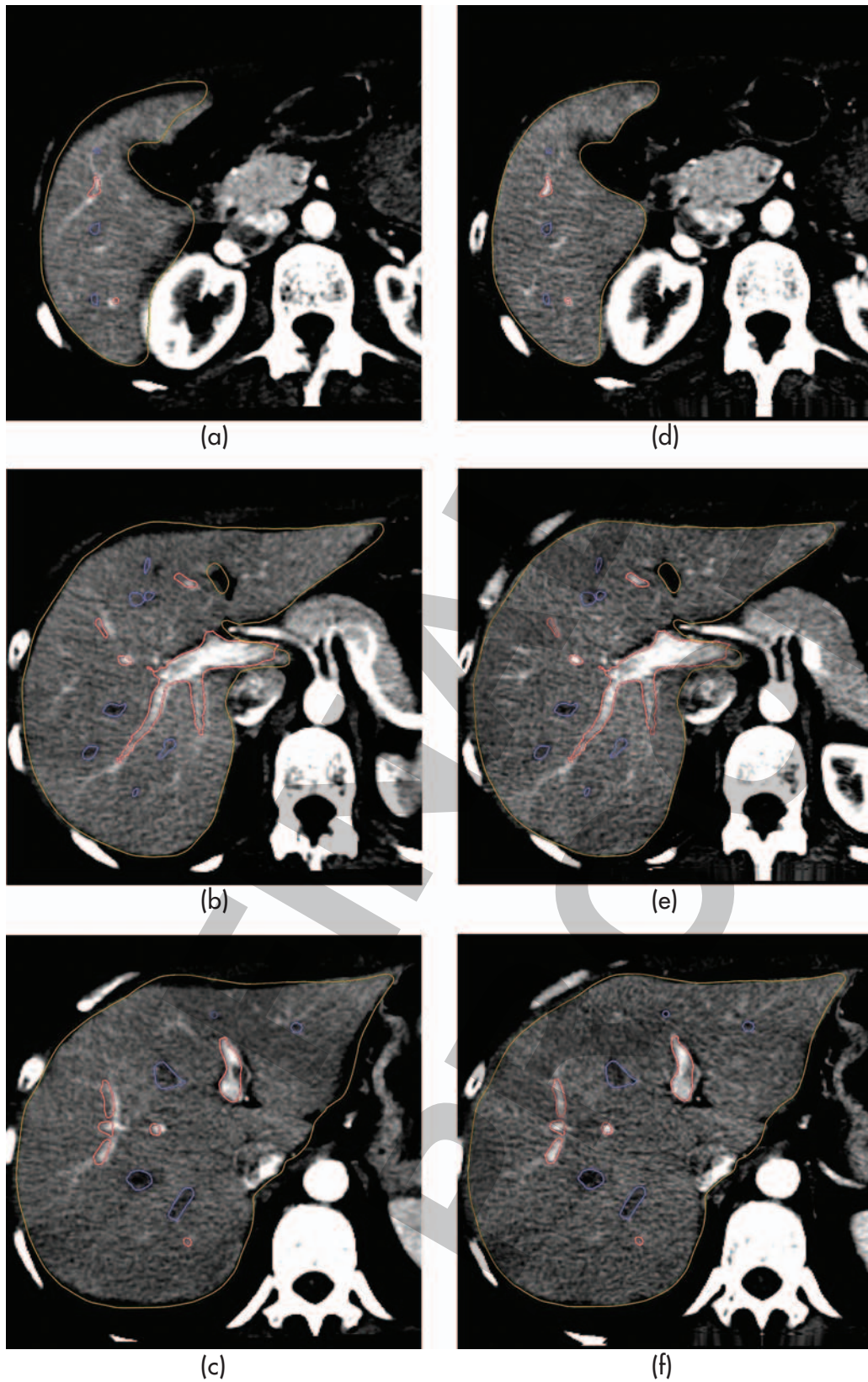


Figure 5 Three different axial slices of the PV phase of data set CT1 with intersecting liver surface (yellow), portal (pink) and hepatic veins (blue) from the HV phase. The left column shows results after rigid registration with masking and the right column after non-rigid registration.

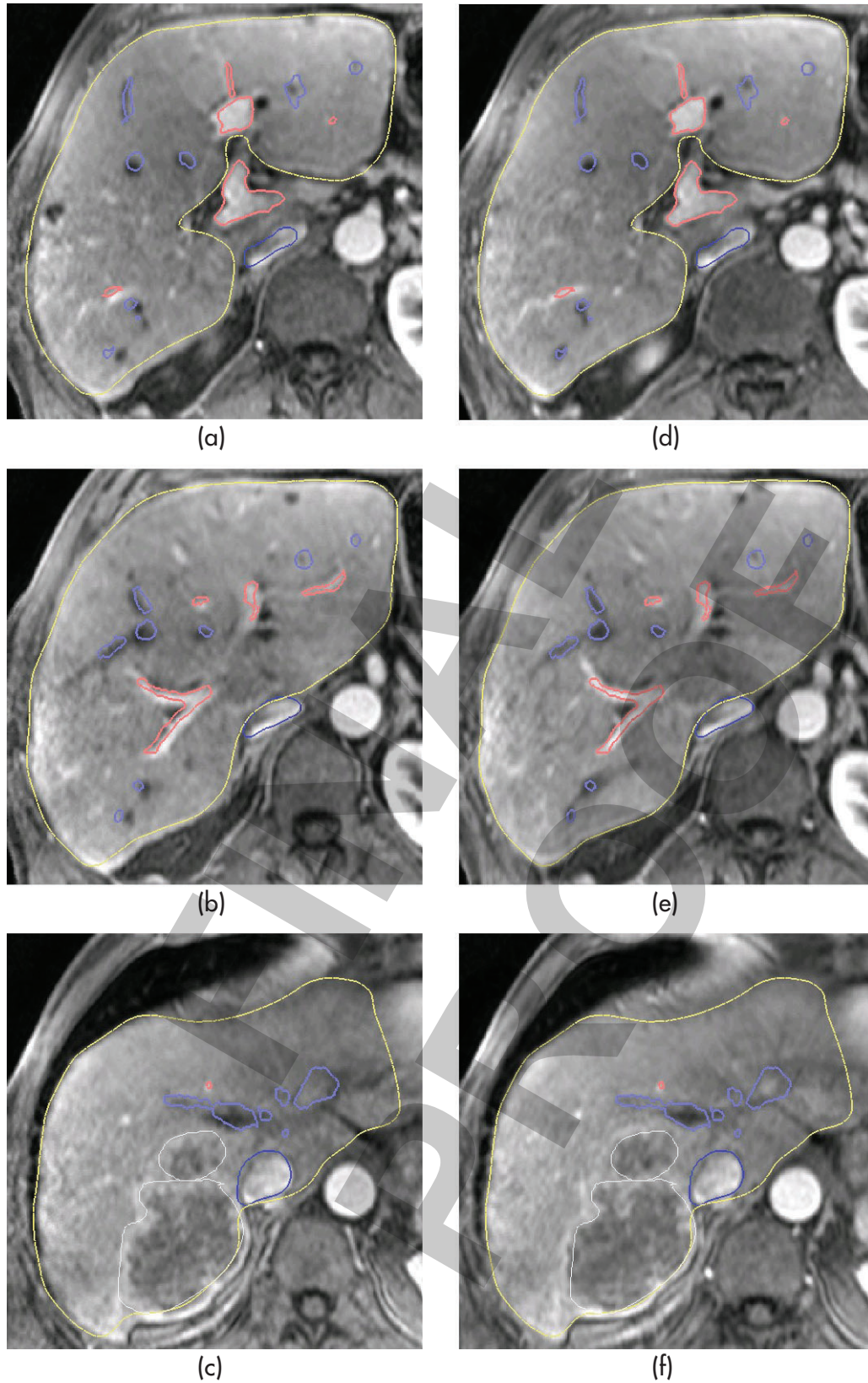


Figure 6 Three different axial slices of the PV phase of data set MR4 with intersecting liver surface (yellow), tumour (white), vena cava (dark blue), portal (pink) and hepatic veins (light blue) of the HV phase. The left column shows results after rigid registration with masking and the right column after non-rigid registration.

Table 1 The RMS distances in mm between differently transformed portal vein centre lines are listed

	CT1	CT2	CT3	CT4	CT5	MR1	MR2	MR3	MR4	MR5	AVG
Initial to rigid masked	9.2	1.4	1.3	3.2	12.3	4.6	7.1	10.0	11.0	11.1	7.2 (+/- 4.2)
Rigid to rigid masked	5.2	1.6	0.7	2.0	3.8	3.5	5.7	5.2	5.6	5.8	3.9 (+/- 1.9)
Rigid masked to non-rigid	3.0	1.6	1.4	1.6	2.8	1.5	2.4	1.9	3.0	2.3	2.2 (+/- 0.6)

The first row specifies the movement of the centre lines between their original position and their position after masked rigid registration. In the second row, differences between rigid registration with and without masking are given. The last row quantifies the centre lines movements between masked rigid and non-rigid registration.

Table 2 The approximated distances between portal vein centre lines extracted from PV and HV phase are shown for three different registration strategies

	RMS (mm)			>2 mm (%)		
	rigid	rigid masked	non-rigid	rigid	rigid masked	non-rigid
CT1	4.8	2.5	2.3	85	46	30
CT5	3.5	3.0	2.5	73	61	34
MR4	5.1	2.8	2.6	92	68	47

The RMS value of the distances as well as the portion of the centre line points showing more than 2 mm distance is listed.

with masking over no masking is confirmed again. Applying non-rigid registration in all three cases further decreases the RMS distances, yet the differences are small. The reason might be related to inaccuracies of the method as discussed in the evaluation method section. Additionally, the distances lie in the range of the slice thickness of 2.0–2.5 mm. Looking at the portion of points having more than 2 mm distance shows a more significant improvement by non-rigid registration.

The implemented intensity inhomogeneity correction of MRI data produces good results. In Figure 7, a MRI slice before and after correction, as well as an intensity profile extracted from this slice is shown. Without intensity correction non-rigid registration fails (Figure 8). MI presumes a statistical dependency between model and reference intensity

values of corresponding anatomical structures. Smooth global intensity inhomogeneities disturb these dependencies. The computation of MI is based on the joint 2D intensity histogram of model and reference data; it contains the proportion of each grey value combination over all voxels belonging to the overlapping regions of the two images. Before intensity correction, the distribution is spread along the diagonal of the histogram, shown in Figure 8c, whereas after correction, it is noticeably clustered, shown in Figure 8d.

Influence of masking

The effect of the liver mask on the registration process is analyzed in more detail for CT data. The first question to be addressed is, whether it is necessary to mask data for rigid registration, if it is

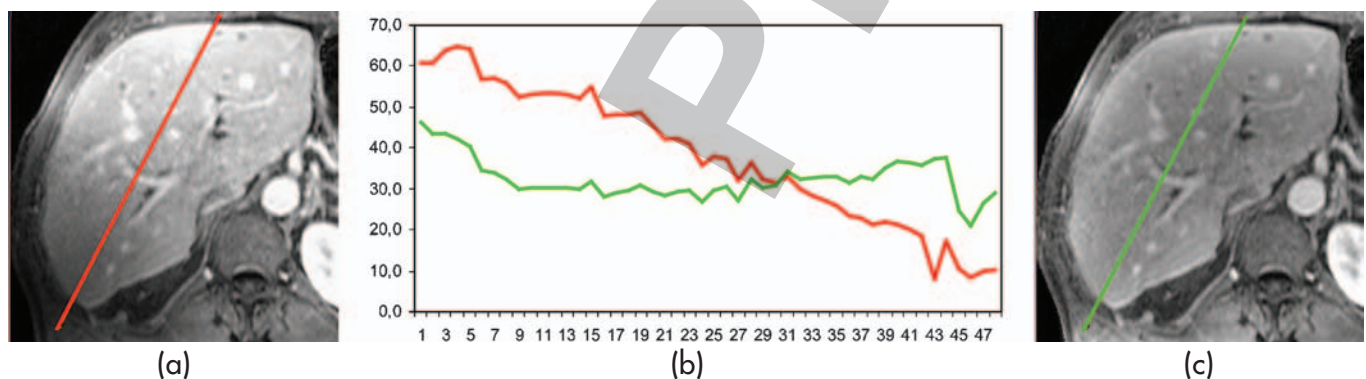


Figure 7 MR image slice without (left) and with inhomogeneity correction (right). The graph in the middle shows a grey value profile of the original (red) and corrected (green) image data. The position of the profile is visualized in the image slice.

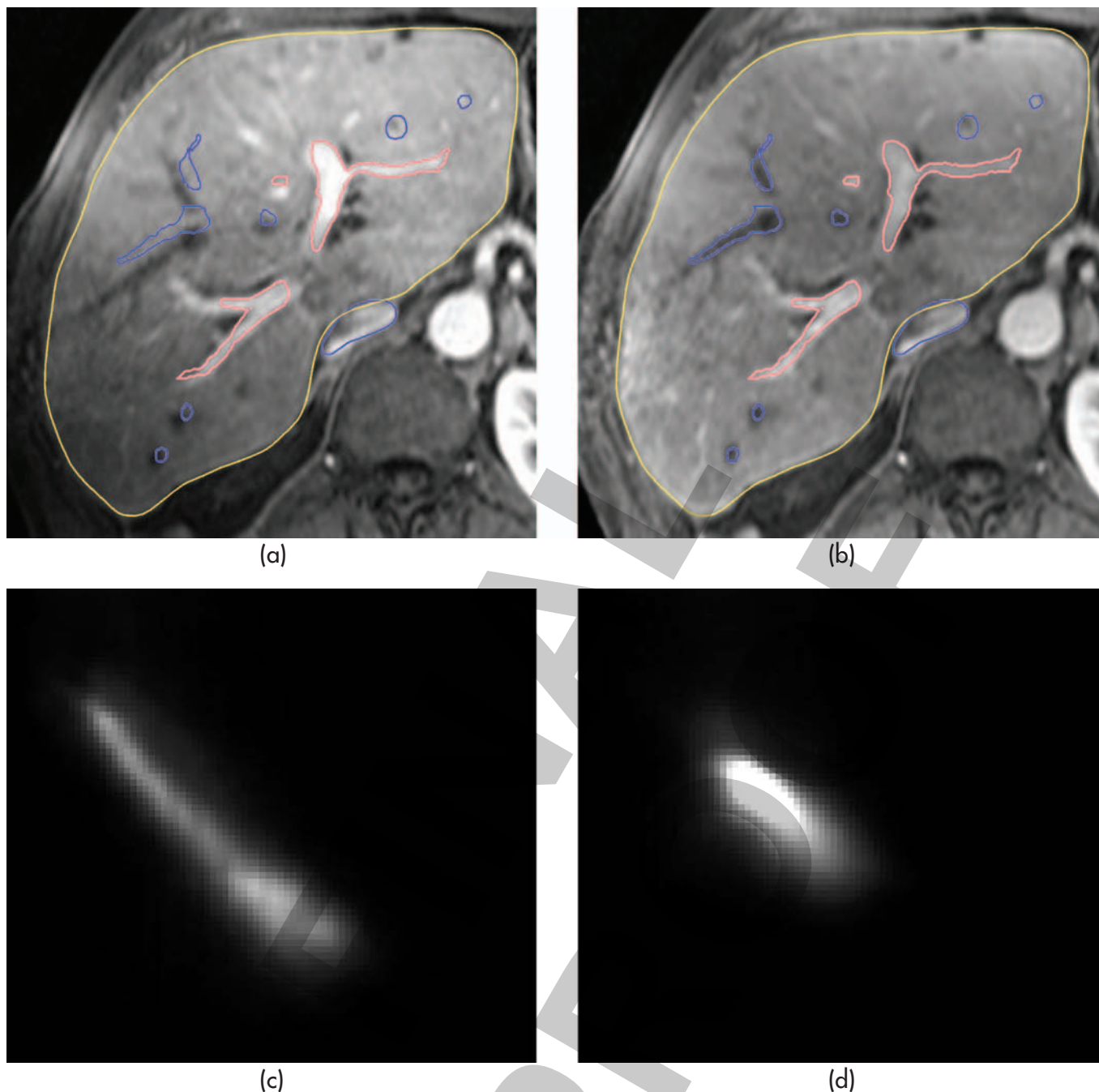


Figure 8 The result of non-rigid registration is shown for original (a) and inhomogeneity corrected (b) MRI data. In figure (c) and (d), the 2D Histogram of the joint intensity value distribution of rigidly registered model and reference MRI data is displayed. On the left, the histogram is shown before intensity inhomogeneity correction and on the right after.

used only as initial registration for the non-rigid method. The answer is no, as can be seen in the first row of Table 3. No significant differences between the resulting non-rigid transformations can be observed visually. The non-rigid registration algorithm adjusts the differences of the two initial rigid transformations. Consequently, no masking has to be applied if it is decided to use non-rigid registration.

Another issue is, whether there is a difference between automatic and manual masking. The automatic adaptation of the liver shape model works well in all but one case (CT5). See Figure 9 for a good and a bad example. The automatic liver masking is not as accurate as the manual, but these deviations only have minor influence on the rigid registration process shown in row 2 of Table 3.

Table 3 The RMS distances in mm between differently transformed portal vein centre lines are listed

	CT1	CT2	CT3	CT4	CT5
Non-rigid with initial rigid and rigid masked	0.8	0.5	0.9	0.7	0.7
Rigid with manual and automatic masking	0.8	0.7	0.9	0.4	1.4

The first row shows the distances of non-rigid transformations resulting from rigidly pre-registered data with and without masking. The second row gives the distances between rigid transformations using manual or automatic masking.



Figure 9 A typical result (CT1) of the automatic masking method is illustrated on the left, and the only bad result is illustrated on the right (CT5).

DISCUSSION AND CONCLUSION

The aim of this contribution is to evaluate existing intensity-based registration algorithms on clinical data for liver surgery planning. The focus is not on the development of new methods. The investigated question is how much the liver's position and shape changes between the portal venous and the hepatic venous phase, and whether these changes can be eliminated by rigid, and if necessary, by non-rigid MI based registration. This study shows that in most cases, patients are not able to reproduce the respiratory state of PV phase in HV phase exactly. Rigid movements and deformations are lower than reported by Rohlfing et al. ⁽⁸⁾ This is not surprising, because they measure the differences between maximal inhale and exhale state, while we only consider different inhale positions.

Masked rigid and non-rigid intensity-based registration is well suited to correct for the displacements of the liver between PV and HV

phase. The key to successful rigid registration of the liver is to restrict evaluation of the MI distance measure to liver voxels. This is also reported by other groups ^(9–11). Since in our case a precise segmentation of the liver for surgery planning is available anyway, liver masking is easy. In cases where there is no manual segmentation provided, we propose to use an automatic segmentation method based on a statistical shape model of the liver. This type of automatic masking produces registration results that are almost identical to the case of manual masking.

For non-rigid registration masking is not necessary. In the case of MR images acquired with a surface coil, intensity inhomogeneities lead to unsatisfactory results after non-rigid registration. Thus Rohlfing et al. decided in an earlier work ⁽²⁹⁾ to use the body coil. However, using the surface coil often is preferred due to its higher signal to noise ratio. We overcome this problem with our

method by performing inhomogeneity corrections based on histogram equalization.

In the future we want to investigate whether additional constraints, like volume preservation^(30, 31), could help to overcome small remaining inaccuracies after non-rigid registration. We think that especially at the periphery of the liver, deformations should follow physical rules to a larger extent. The next important step to take is to quantify the impact of more precise vessel models on the preoperative planning process.

Rigid registration with automatic masking achieves fast and in many cases acceptable registration results. In cases where higher accuracies are desired non-rigid registration must be applied.

REFERENCES

- Preim B, Bourquian H, Selle D, Peitgen HO, Oldhafer KJ. Resection Proposals for Oncologic Liver Surgery based on Vascular Territories. In: Lemke HU, Vannier MW, Inamura K, and Farman AG, editors. *Computer Assisted Radiology and Surgery*. Springer; 2002. p. 353–8.
- Lange T, Eulenstein S, Hunerbein M, Schlag PM. Vessel-based non-rigid registration of MR/CT and 3D ultrasound for navigation in liver surgery. *Comput Aided Surg*. 2003;8(5):228–40.
- Lange T, Eulenstein S, Hünerbein M, Lamecker H, Schlag PM. Augmenting Intraoperative 3D Ultrasound with Preoperative Models for Navigation in Liver Surgery. In: Barillot C, Haynor DR, and Hellier P, editors. *Medical Image Computing and Computer-Assisted Intervention*. Vol. 3217, Lecture Notes in Computer Science, Springer; 2004. p. 534–41.
- Selle D, Preim B, Schenk A, Peitgen HO. Analysis of vasculature for liver surgical planning. *IEEE Trans Med Imaging*. 2002;21(11):1344–57. doi: 10.1109/TMI.2002.801166
- Meinzer HP, Thorn M, Cardenas C. Computerized planning of liver surgery - an overview. *Computers & Graphics*. 2002; 26(4):569–76. doi: 10.1016/S0097-8493(02)00102-4
- Soler L, Delingette H, Malandain G, Montagnat J, Ayache N, Koehl C, Dourthe O, Malassagne B, Smith M, Mutter D, Marescaux J. Fully automatic anatomical, pathological and functional segmentation from CT scans for hepatic surgery. *Comput Aided Surg*. 2001;21(11):1344–1357.
- Reitinger B, Bornik A, Beichel R, Werkgartner G, Spindler W. Tools for Augmented Reality based Liver Resection Planning. In: *Proceedings of the SPIE Medical Imaging 2004: Visualization, Image-guided Procedures, and Display*. 2004. p. 88–99.
- Rohlfing T, Maurer CR, Jr., O'Dell WG, Zhong J. Modeling liver motion and deformation during the respiratory cycle using intensity-based nonrigid registration of gated MR images. *Med Phys*. 2004;31(3):427–432. doi: 10.1118/1.1644513
- Carrillo A, Duerk JL, Lewin JS, Wilson DL. Semiautomatic 3-D image registration as applied to interventional MRI liver cancer treatment. *IEEE Trans Med Imaging*. 2000;19(3): 175–85. doi: 10.1109/42.845176
- van Dalen JA, Vogel W, Huisman HJ, Oyen WJG, Jager GJ. Accuracy of rigid CT-FDG-PET image registration of the liver. *Phys Med Biol*. 2004;49:5393–5405. doi: 10.1088/0031-9155/49/23/014
- Park H, Blend PH, Balter J, Meyer CR. Method for Quantifying Lesion Change from Interval Liver Examinations. In: *International Workshop on Growth and Motion in 3D Medical Images*. 2002.
- Charnoz A, Agnus V, Soler L. Portal Vein Registration for the Follow-Up of Hepatic Tumours. In: Barillot, C., Haynor DR, and Hellier P, editors. *Medical Image Computing and Computer-Assisted Intervention*. Vol. 3216, Lecture Notes in Computer Science, Springer; 2004. p. 878–86.
- Aylward SR, Jomier J, Weeks S, Bullitt E. Registration and Analysis of Vascular Images. *International Journal of Computer Vision*. 2003;55(2–3):123–38. doi: 10.1023/A:1026126900358
- Modersitzki J. *Numerical Methods for Image Registration*. Oxford University Press; 2004.
- Rueckert D, Sonoda LI, Hayes C, Hill DL, Leach MO, Hawkes DJ. Nonrigid registration using free-form deformations: application to breast MR images. *IEEE Trans Med Imaging*. 1999;18(8):712–21. doi: 10.1109/42.796284
- Meyer CR, Boes JL, Kim B, Bland PH. Demonstration of accuracy and clinical versatility of mutual information for automatic multimodality image fusion using affine and thin-plate spline warped geometric deformations. *Med Image Anal*. 1997;1(3):195–206. doi: 10.1016/S1361-8415(97)85010-4
- Fischer B, Modersitzki J. A unified approach to fast image registration and a new curvature based registration technique. *Linear Algebra and its Applications*. 2004;380:107–124. doi: 10.1016/j.laa.2003.10.021
- Bajcsy R, Kovacic S. Multiresolution elastic matching. *Computer Vision, Graphics and Image Processing*. 1989;46: 1–21.
- Christensen GE. *Deformable shape models for anatomy [dissertation]*. Sever Institute of Technology, Washington University; 1994.
- Studholme C, Hill DL, Hawkes DJ. Automated three-dimensional registration of magnetic resonance and positron emission tomography brain images by multiresolution optimization of voxel similarity measures. *Med Phys*. 1997;24(1):25–35. doi: 10.1118/1.598130
- Cootes T, Hill A, Taylor CJ, Haslam J. Use of active shape models for locating structures in medical images. *Image and Vision Computing*. 1994;12:355–66. doi: 10.1016/0262-8856(94)90060-4
- Lamecker H, Lange T, Seebass M. A Statistical Shape model for the liver. In: Dohi T and Kikinis R, editors. *Medical Image Computing and Computer-Assisted Intervention*. Vol. 2489, Lecture Notes in Computer Science, Springer; 2002. p. 422–7.
- Lamecker H, Lange T, Seebass M, Eulenstein S, Westerhoff M, Hege HC. Automatic Segmentation of the Liver for the Preoperative Planning of Resections. In: Westwood JD and et al., editors. *Medicine Meets Virtual Reality*. Vol. 94, Studies in Health Technologies and Informatics, IOS Press; 2003. p. 171–4.
- Lamecker H, Lange T, Seebass M. Segmentation of the Liver using a 3D Statistical Shape Model. *Zuse Institute Berlin. ZIB Technical Report 04–09*; 2004.
- Rohlfing T, Maurer CR, Jr. Nonrigid image registration in shared-memory multiprocessor environments with application to brains, breasts, and bees. *IEEE Trans Inf Technol Biomed*. 2003;7(1):16–25. doi: 10.1109/TITB.2003.808506

- 26 Stalling D, Westerhoff M, Hege HC. Amira: A Highly Interactive System for Visual Data Analysis. In Hansen CD, Johnson CR (eds). *The Visualization Handbook*. Elsevier; 2005:749–67.
- 27 Likar B, Viergever MA, Pernus F. Retrospective Correction of MR Intensity Inhomogeneity by Information Minimization. In: Delp SL, DiGioia AM, and Jaramaz B, editors. *Medical Image Computing and Computer Assisted Intervention*. Vol. 1935, Springer; 2000. p. 375–84.
- 28 Sato M, Bitter I, Bende M, Kaufmann A, Nakajima M. TEASAR: Tree-structure extraction algorithm for accurate and robust skeletons. In: *Proceedings of the 8th Pacific Graphics Conference on Computer Graphics and Application (PACIFIC GRAPHICS-00)*. 2000. p. 281–9. doi: 10.1109/PCCGA.2000.883951
- 29 Rohlfing T, Maurer CR, O'Dell WG, Zhong J. Modeling liver motion and deformation during the respiratory cycle using intensity-based free-form registration of gated MR images. In: Mun SK, editors. *Proceedings of the SPIE*. Vol. 4319, 2001. p. 337–48. doi: 10.1117/12.428073
- 30 Rohlfing T, Maurer CR, Jr., Bluemke DA, Jacobs MA. Volume-preserving nonrigid registration of MR breast images using free-form deformation with an incompressibility constraint. *IEEE Trans Med Imaging*. 2003;22(6):730–41. doi: 10.1109/TMI.2003.814791
- 31 Haber E, Modersitzki J. Volume Preserving Image Registration. In: Barillot, C., Haynor DR, and Hellier P, editors. *Medical Image Computing and Computer-Assisted Intervention*. Vol. 3216, *Lecture Notes in Computer Science*, Springer; 2004. p. 591–8.

FINAL
PROOF